Requirements for Specific Binding of Low Affinity Inhibitor Fragments to the SH2 Domain of ^{pp60}Src Are Identical to Those for High Affinity Binding of Full Length Inhibitors

Gudrun Lange,*[†,§] Dominique Lesuisse,[‖] Pierre Deprez,[‡] Bernard Schoot,[‡] Petra Loenze,[†] Didier Bénard,[‡] Jean-Pierre Marquette,[‡] Pierre Broto,[‡] Edoardo Sarubbi,[‡] and Eliane Mandine[‡]

Aventis Pharma, 102 route de Noisy, 93235 Romainville, France, and Aventis Pharma, Structural Biology, 65926 Frankfurt, Germany

Received June 18, 2002

Results from a novel approach which uses protein crystallography for the screening of a low affinity inhibitor fragment library are analyzed by comparing the X-ray structures with bound fragments to the structures with the corresponding full length inhibitors. The screen for new phospho-tyrosine mimics binding to the SH2 domain of ^{pp60}src was initiated because of the limited cell penetration of phosphates. Fragments in our library typically had between 6 and 30 atoms and included compounds which had either millimolar activity in a Biacore assay or were suggested by the ab initio design program LUDI but had no measurable affinity. All identified fragments were located in the phospho-tyrosine pocket. The most promising fragments were successfully used to replace the phospho-tyrosine and resulted in novel nonpeptidic high affinity inhibitors. The significant diversity of successful fragments is reflected in the high flexibility of the phospho-tyrosine pocket. Comparison of the X-ray structures shows that the presence of the H-bond acceptors and not their relative position within the pharmacophore are essential for fragment binding and/or high affinity binding of full length inhibitors. The X-ray data show that the fragments are recognized by forming a complex H-bond network within the phospho-tyrosine pocket of SH2. No fragment structure was found in which this H-bond network was incomplete, and any uncompensated H-bond within the H-bond network leads to a significant decrease in the affinity of full length inhibitors. No correlation between affinity and fragment binding was found for these polar fragments and hence affinity-based screening would have overlooked some interesting starting points for inhibitor design. In contrast, we were unable to identify electron density for hydrophobic fragments, confirming that hydrophobic interactions are important for inhibitor affinity but of minor importance for ligand recognition. Our results suggest that a screening approach using protein crystallography is particularly useful to identify universal fragments for the conserved hydrophilic recognition sites found in target families such as SH2 domains, phosphatases, kinases, proteases, and esterases.

Introduction

Traditionally, structure-based drug design plays a major role in the optimization of hits found by high throughput screening of company-owned libraries or derived from other sources. More recently it has emerged that particularly for targets involving protein−protein interactions, there is a high probability of not finding a promising hit by high throughput screening,[1] and alternative approaches for lead generation are required.

With no hits available, computer programs have been used to generate leads for structure-based drug design. These approaches range from programs such as DOCK[2] and FLExX[3] which dock full length inhibitors into putative binding sites and programs such as GRID[4] which scan a putative binding site using probes representing H-bond donors/acceptors or hydrophobic elements in order to identify H-bond partner positions in the binding pocket and evaluate the size of hydrophobic pockets. Somewhat between, there are programs such as LUDI[5] which selects fragments from a virtual database and places them into the binding pocket. Connecting these fragments ideally results in a full length inhibitor. However, these approaches have not always been successful, possibly due to the limited quality of potentials and scoring functions used. In addition, the flexibility of the protein is not taken into account since it is unknown to which extent the protein will adapt to the ligand.

So far, only a few experimental protein structure-based approaches for lead generation have been reported. They include NMR measurement of the target protein mixed with inhibitor fragments.[6,7] On the basis of the difference in the NMR spectra of free and complexed protein, inhibitor fragments are identified which bind to pockets in the target protein (SAR by NMR). Recently, it has been demonstrated that screen-

* To whom correspondence should be addressed: Industriepark Höchst, Building G837, Tel.: +49-69-30516207, Fax: +49−69−305−17768, Email: gudrun.lange@Bayercropscience.com.
[†] Aventis Pharma, Frankfurt, Germany.
[‡] Aventis Pharma, Romainville, France.
[§] Present address: Bayer CropScience, Chemistry, 65926 Frankfurt, Germany.
[‖] Present address: Aventis Research Centre, 13 Quai Jules Guesde, 94403 Vitry, France.

10.1021/jm020970s CCC: $25.00
Published on Web 10/28/2003

ing of a fragment library using protein crystallography can be used for lead generation.[8,9] Inhibitor fragments are soaked into the binding pocket of the crystallized protein and—in case of specific binding—the corresponding X-ray structures are determined. Starting from the high-resolution structure of a protein−fragment complex, a full length inhibitor can be obtained by attaching an inhibitor scaffold designed by structure-based drug design. Alternatively, libraries can be screened to replace fragments in already existing full length inhibitors.[9] These replacements can be selected in order to modify a variety of features such as binding affinity, cell penetration, solubility, or selectivity. However, using protein crystallography only a limited number of compounds can be investigated and thus either compound cocktails were used[8] or affinity-based filtering techniques[9] were applied.

Understanding the key principles according to which fragments bind to proteins would allow us to limit the experimental screening to fragment candidates which have a high likelihood of binding to the protein. A comparison between X-ray structures with bound fragments to those with full length inhibitors should allow us to extract some general rules according to which low affinity fragments bind to proteins. In addition, the superposition of a multitude of X-ray structures with different inhibitor fragments would reveal at which positions within the binding site specific functional groups such as H-bond donors/acceptors or hydrophobic groups are required. If a binding site is rigid, the positions of functional groups should form well-defined clusters in such a superposition of experimental structures. However, for flexible ligand binding sites, there is additional information encoded in the size and shape of the clusters for a given functional group. The topology of the individual clusters and their relative position will reflect the flexibility of the protein and show to what extent the protein can stretch itself in order to accommodate a ligand into the binding site.

Herein, we analyze our results of the screening of inhibitor fragments[9] using a combination of a Biacore-based assay, computer predictions, and protein crystallography for the design of inhibitors of the SH2 domain of pp60src. On the basis of this analysis, more general requirements for the binding of low affinity fragments and thus for a successful application of this novel methods will be proposed. pp60src kinase has been implicated in bone resorption and represents a potential target for therapeutic intervention of osteoporosis.[10] Crystals structures of peptides show that there are two major binding sites: a positively charged phosphotyrosine binding site and the hydrophobic pY+3 pocket.[11] So far, few inhibitors have been described which combine a nonpeptidic character with an affinity comparable to the natural substrate pYEEI. Combining the approach described above with traditional structure-based lead optimization[12−15] has resulted within little more than a year in nonpeptidic inhibitors with IC_{50} values in the low nanomolar range.

Materials and Methods

Protein Crystallography. Human pp60src SH2 was purified and crystallized as described earlier.[9] The crystals were soaked overnight with the corresponding compound solution and prior to data collection with 10% of glycerol as cryoprotectant. Most data were collected at −170 °C on either a Mar345 imaging system or a MarCCD mounted on a rotating anode X-ray generator (GX21, Enraf Nonius). Some data were collected at beam-lines at the ESRF or Lure. The data were processed using XDS[16] and refined using X-PLOR[17] based on a model provided by Ariad. Model building and structure comparison was carried out using Quanta.[18] Prior to their comparison, all structures were superimposed using LSQKAB.[19] The LUDI[5] predictions were based on 1shd[20] and calculated using standard parameters. The compounds including the most important details of the data collection and structure refinement and their IC_{50} value are listed in Charts 1 and 2. The IC_{50} values of compounds **1**−**10** were measured as described earlier using either Surface Plasmon Resonance (SPR) or Scintillation Proximity Assay.[9] The X-ray structures (PDB codes 1o41, 1o42, 1o43, 1o44, 1o45, 1o46, 1o47, 1o48, 1o49, 1o4A, 1o4B, 1o4C, 1o4D, 1o4E, 1o4F, 1o4G, 1o4H, 1o4I, 1o4J, 1o4K, 1o4L, 1o4M, 1o4N, 1o4O, 1o4P, 1o4Q,1o4R,1o4S) have been deposited at the Protein Data Bank.

Syntheses. The synthesis of compound **1** is described in reference.[13] The synthesis of compounds **2, 3**, and **6** is described in reference.[9] The synthesis of compounds **5**, **7**, and **8** is described in reference.[21,22] Compounds **4** and **9** have not been published, and their synthesis will be reported here.

Starting malonate **11** was fluorinated using *N*-fluorobenzenesulfonimide in the presence of potassium hexamethyldisilyl azide at low temperature. The resulting fluoro-malonate **12** was condensed with methyl-2-acetamidoacrylate using Heck conditions yielding the ester **13a**, which was saponified using lithium hydroxide as a base to generate the acid **13b**. Condensation of the resulting dehydrotyrosine analogue **13b** with the azepinone **14** afforded **15**, which was subsequently hydrogenated on palladium and saponified using formic acid to yield **4** (Scheme 1).

The same azepinone **14** was condensed with 3-[3,4-bis(diethoxyphosphoryl)phenyl-2-*tert*-butoxycarbonylaminopropionic acid **17** synthesized according to W. Shakespeare[23] to afford the diphosphono derivative **18**. The latter was deprotected using trifluoroacetic acid yielding the amine **19a** which was subsequently acetylated in pyridine to give the acetamide **19b**. The resulting diphosphono ester **19b** was deprotected using trimethylsilyl iodide to provide the final diphosphonic acid **9** (Scheme 2).

Results

A fragment library was generated which included 150 compounds typically consisting of 6−30 atoms. The compounds were either commercially available or were part of small libraries prepared by parallel synthesis. To reduce the number of compounds to a feasible amount for the crystallographic experiments, a Biacore assay was used as a filter. Phenyl phosphate, the smallest fragment of the substrate pYEEI with a detectable binding affinity for Src SH2, was used as a reference. Fragments that displayed comparable or better binding affinity than phenyl phosphate were kept for soaking. In addition, fragments suggested by the

Chart 1. Chemical Structure and IC_{50} Values of Fragments

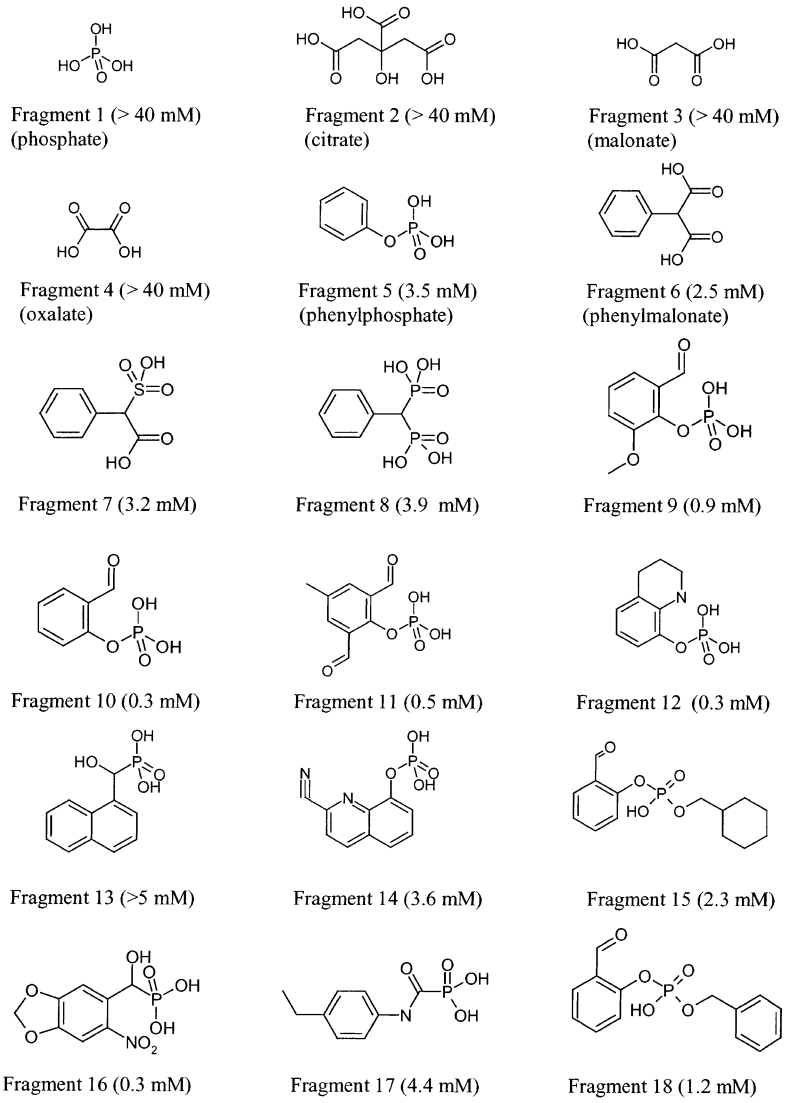

program LUDI were included. These fragments showed no biochemical activity within the range measured. The citrate fragment was found bound to the protein after a citrate buffer had been used during purification and displayed no measurable affinity. The successfully soaked fragments including their IC_{50} values are listed in Chart 1.

Soaking of *src* SH2 crystals was tried for about 200 compounds including fragments and full length inhibitors. Since soaking is a fast but not always reliable method, phenyl phosphate was used as an internal standard. A total of 200 X-ray data sets including both fragments and full length inhibitors were collected and analyzed resulting in a total of 45 structures with bound inhibitor fragments or full length inhibitors. They included two structures with fragments predicted by LUDI and 14 structures with fragments found using the Biacore assay. All X-ray structures were better than 2.1 Å and refined to *R*-factors below 20%. The electron density was for all structures well defined, though some compounds displayed limited local disorder.

Our general experience was that soluble fragments with a substantial number of putative H-bond partners had a fairly good chance to bind in a specific binding mode. Except for phenyl phosphate which was clearly bound at two sites, all other fragments were bound only in the phospho-tyrosine pocket and are, therefore, phospho-tyrosine mimics. The fragments identified differed significantly in their chemical nature and include oxalate, malonate, phenylmalonate, sulfates, and various compounds from an aldehyde library. We did not observe well-defined electron density for the more hydrophobic fragments predicted by LUDI which were tried in order to identify inhibitor fragments pointing into the hydrophobic pY+3 pocket. This may be due to either the limited solubility of the compounds and/or an undefined positioning within the pocket. No correlation between affinity and fragment binding was found for the polar ligands. Two fragments out of six suggested by LUDI were found to bind in the corresponding soaking experiments.[9] However, the predicted binding modes for oxalate and malonate was not confirmed in the experiments. Figure 1 shows the electron density of a selection of nine fragments binding into the phospho-tyrosine pocket. The maps were calculated using only coordinates of the protein model and omitting the coordinates of the fragments (omit maps).

Chart 2. Chemical Structure and IC_{50} Values of Inhibitors

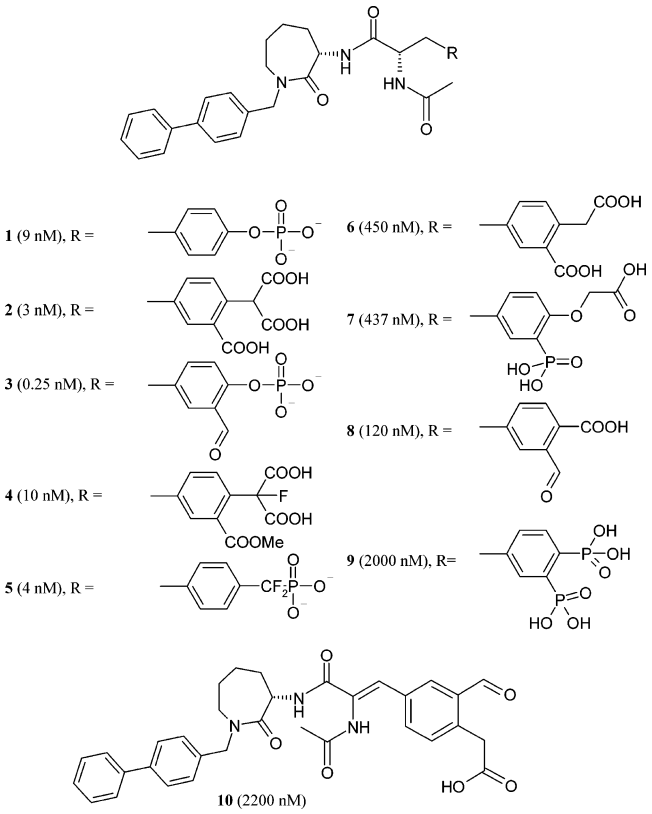

The superposition of the fragment structures shows that the protein in all structures superimposes excellent with rms deviations of typically 0.2 Å for most main chain atoms. However, closer inspection reveals that there are significant differences in the phospho-tyrosine pocket (Figure 2a). The conformational changes induced upon binding of the individual fragments result in differences of up to 3 Å for the position of identical protein atoms in different structures. For instance, comparison of the oxalate and malonate structures shows that both fragments interact in an identical manner. In both structures, one carboxylate moiety interacts with the side chains of R14 and R34 and the main chain nitrogen of E37 while the second carboxylate moiety forms H-bonds to the side chains of S36, T38, and the main chain nitrogen of T38 (Figure 2b). The positions of protein H-bond donors (R14NH2, R34NH2, and E37N) interacting with the first carboxylate moiety are identical within the experimental error. However, the positions of the protein H-bond donors interacting with the second carboxylate moiety differ significantly in both structures i.e., 0.6 Å for S36OG, 1.1 Å for T38N, and 2.6 Å for T36OG.

A closer analysis of the superimposed structures shows that the loop consisting of amino acids 36−42 displays a significant flexibility. The structure of this loop is stabilized by H-bonds between the backbone amides of S36 and A42 and backbone carbonyls of A42 and T39, respectively. In addition, the side chain of S36 interacts via its two free electron pairs with the amide backbones of T38 and T39 while the proton of S36OG acts in all fragment structures as an H-bond donor to the fragment. This means, that a rotation of the serine side chain induces a conformational change of the loop 36−42. The difference of 20° between the chi-values of S36OG found in the oxalate and the malonate structure results in the considerable differences in loop conformation described above. The observed differences for corresponding cα position in the malonate and oxalate structure are 0.45 Å for T37, 1.69 Å for T38, and 0.39 Å for N39 which is well above the coordinate error. For other ligands, the observed conformation of this loop does not dependent on the size or the affinity of the particular ligand. However, it seems that a loop conformation is assumed which allows the system to complete the H-bond network, and thus the loop conformation depends on the relative positions of H-bond partners within the ligand.

The requirements for specific binding which need to be met by putative millimolar fragments can be extracted from the superposition of all fragment structures. The superposition of the fragment H-bond acceptors (Figure 2c) based on the structure with bound citrate shows that these acceptors form well-defined clusters when interacting with rigid H-bond donors such as R34. However, the cluster formed by the H-bond acceptors to S36OG is quite diffuse, indicating that the exact location of the H-bond partner of S36OG within the phospho-tyrosine pockets is less crucial. The distances of up to 3 Å between individual cluster members reflect the extent of the hinge movement which can be exercised by the side chain of S36. A closer inspection of the fragment binding reveals that in all cases complex H-bond networks are formed between the fragments and SH2 as seen in Figure 2d for the citrate structure. All networks are identical in the rigid part of the pocket and include H-bonds/salt-bridges between the fragments and the side chains of R14, R34, and the backbone amide of E37. In addition, an H-bond between the fragments and S36OG is present in all structures. The details of the individual networks involving the more flexible protein H-bond partners such as T38OG, T39OG, K62NH2, and the backbone amide of T38 differ somewhat and include in some cases a well defined water molecule. However, there are no uncompensated H-bonds neither within the protein nor within the fragment. Hydrophobic interactions seem to be of minor importance at this site since fragments such as citrate and malonate, which have no hydrophobic groups, were unambiguously bound to the protein. However, if different binding modes are accessible to the fragment, additional hydrophobic interactions influence which mode is assumed. For example, the phenyl phosphate fragment binds in a different mode to the phospho-tyrosine in the peptide structures. In both modes the requirements with respect to the H-bond network are fully met but additional hydrophobic interaction—inaccessible in the peptide complexes—favor an alternate binding mode of the phenyl phosphate fragment. Both binding modes have been found subsequently in complex structures with full length inhibitors.[15]

In parallel to the identification of fragments pointing into the phospho-tyrosine pocket, a nonpeptidic inhibitor containing a phospho-tyrosine unit was designed and optimized.[14] The best phospho-tyrosine inhibitor had an activity of 9 nM (inhibitor 1). Subsequently, replacements for the phospho-tyrosine were selected based on the X-ray structures of the fragments. In particular,

Scheme 1

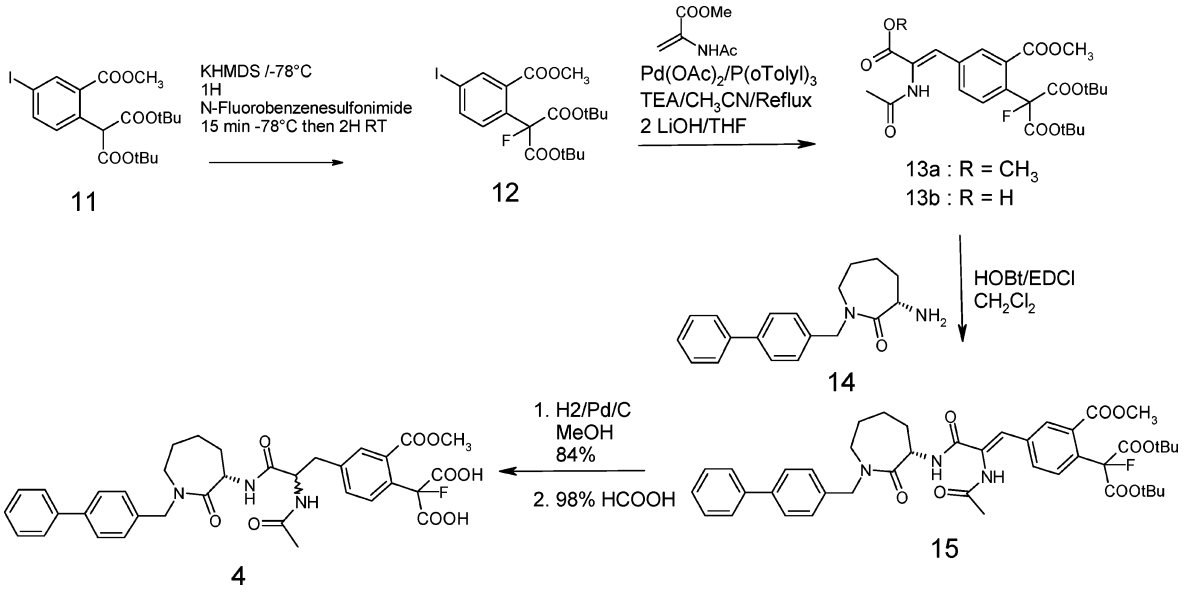

Scheme 2

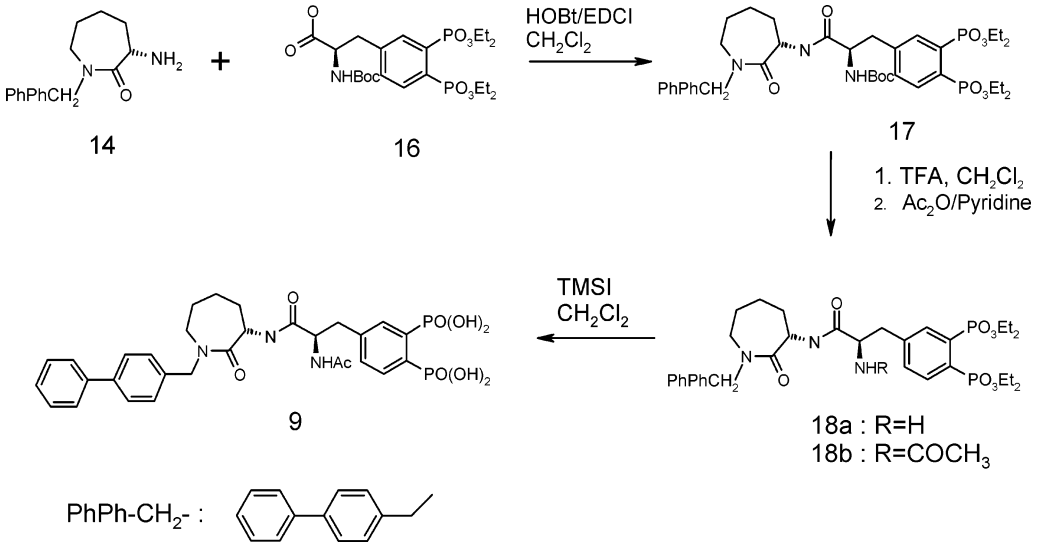

different phenyl malonate fragments incorporating the structural information obtained from the malonate and citrate complexes were designed and subsequently tested in the Biacore assay. Replacement of phosphotyrosine by 2-carboxy phenyl malonate resulted in an inhibitor with an IC_{50} value of 3 nM (inhibitor 2). The omit-map displaying the electron density for inhibitor 2 is shown in Figure 3a. The structures of the complexes with inhibitor 1 and 2 including their common inhibitor atoms superimpose extremely well (Figure 3b). As expected, there are some changes within the phosphotyrosine pocket due to the different induced fit of the phospho-tyrosine and 2-carboxy phenyl malonate fragment. Comparison of the X-ray structures containing the fragment with that containing inhibitor **2** (Table 1) shows that the malonate, citrate, and phenyl malonate fragments had the same binding mode as the corresponding group in inhibitor 2, indicating that the fragments were bound in a mode relevant for drug design (Figure 4a−c). The protein structures including the H-bond acceptors in inhibitor 2 and in the fragments superimpose within the experimental error. In particular, the distances between corresponding H-bond acceptors in the structures of inhibitor 2 and citrate were between 0.2 and 0.4 Å.

Further analysis of complex structures with full length inhibitors showed that the requirements for fragment binding are identical to those for high affinity full length inhibitors. The phospho-tyrosine fragment in inhibitor 1 was replaced by other putative mimics, and subsequently the crystal structures of some interesting inhibitors, 3−10, were determined. The affinity of inhibitors 1−10 differs by several orders in magnitude, i.e., between micromolar and picomolar. The superposition of the fragment and full length inhibitor structures shows that the common atoms interact identically within the SH2 domain (Figure 5a). Thus, the differences in affinity can be correlated with the different interactions of the inhibitors with the phosphotyrosine pocket.

The positions of all H-bond acceptors in full length inhibitors superimposed based on the protein structure of inhibitor 2 shows that most of the H-bond acceptors of the fragments and full length inhibitors are located

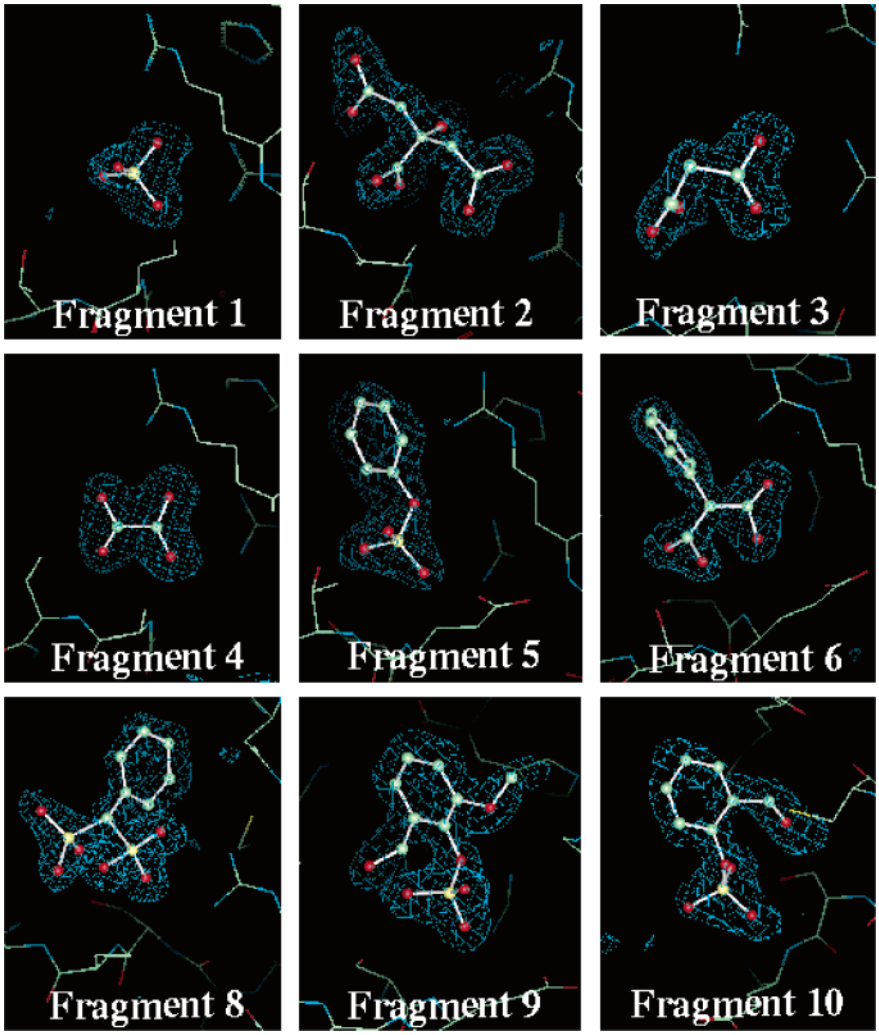

Figure 1. Omit electron density maps of fragments bound to the SH2 domain of *src* contoured at 3σ.

within the clusters defined by the fragments structures (Figure 5b). In particular, the H-bond acceptors of high affinity inhibitors are located well within these clusters and form a complete H-bond network with the phosphotyrosine pocket. In contrast, in complexes with poor inhibitors such as 6 or 7 the central H-bond to the side chain of S36 is not made. The importance of this particular H-bond is highlighted by the presence of a second conformation of the phenyl acetic acid moiety in the complex structure with compound **6**. In one conformation, the carboxylic group interacts as expected with R14 and R34. In the second, much lower occupied conformation (10−20%), the H-bond to S36OG is made.[9] In other complex structures with low affinity inhibitors, the electron density of the phospho-tyrosine replacement is disordered even though the electron density of the common inhibitor part is well defined.[15] In these cases, the H-bond acceptors are not located within the clusters defined by the fragments and are thus unable to complete the H-bond network. Examples include inhibitor 9 and 10 with an IC_{50} of 2000 and 2200 nM.

In summary, fragments are bound specific and represent high affinity phospho-tyrosine mimics if their H-bond acceptors are located within the limits highlighted by the fragment H-bond acceptors and thus able to complete the H-bond network present in the phosphotyrosine pocket.

Discussion

The lack of promising hits after high throughput screening of huge compound libraries has intensified the interest in fragment-based approaches using computer algorithms, SAR by NMR or crystallography and cooperative combinatorial chemistry for fragment combination. For instance, it has been demonstrated, that a combination of two weakly binding fragments from a combinatorial library can result in a nanomolar inhibitor.[24] Recently, it has been shown that a screening procedure using protein crystallography can identify new lead compounds and that their X-ray structures form an excellent basis for the design of high affinity inhibitors.[8,9] In addition, we have shown, that fragment libraries can be screened in order to identify replacements such as phospho-tyrosine mimics for already existing inhibitors.[9] Compared to NMR, protein crystallography has less high-throughput potential since collecting a complete data set takes in our case about 6 h at a home source and 10 min at a synchrotron source, and we have been able to finalize two structures per day. This lack has been compensated for by either using a cocktail of compounds[8] or by filtering the fragment library using a biacore assay.[9] Also fragments found by other techniques such as mass spectrometry,[25] NMR experiments,[5,26] and in particular computer prediction[27] can be used as input for crystallographic screening.

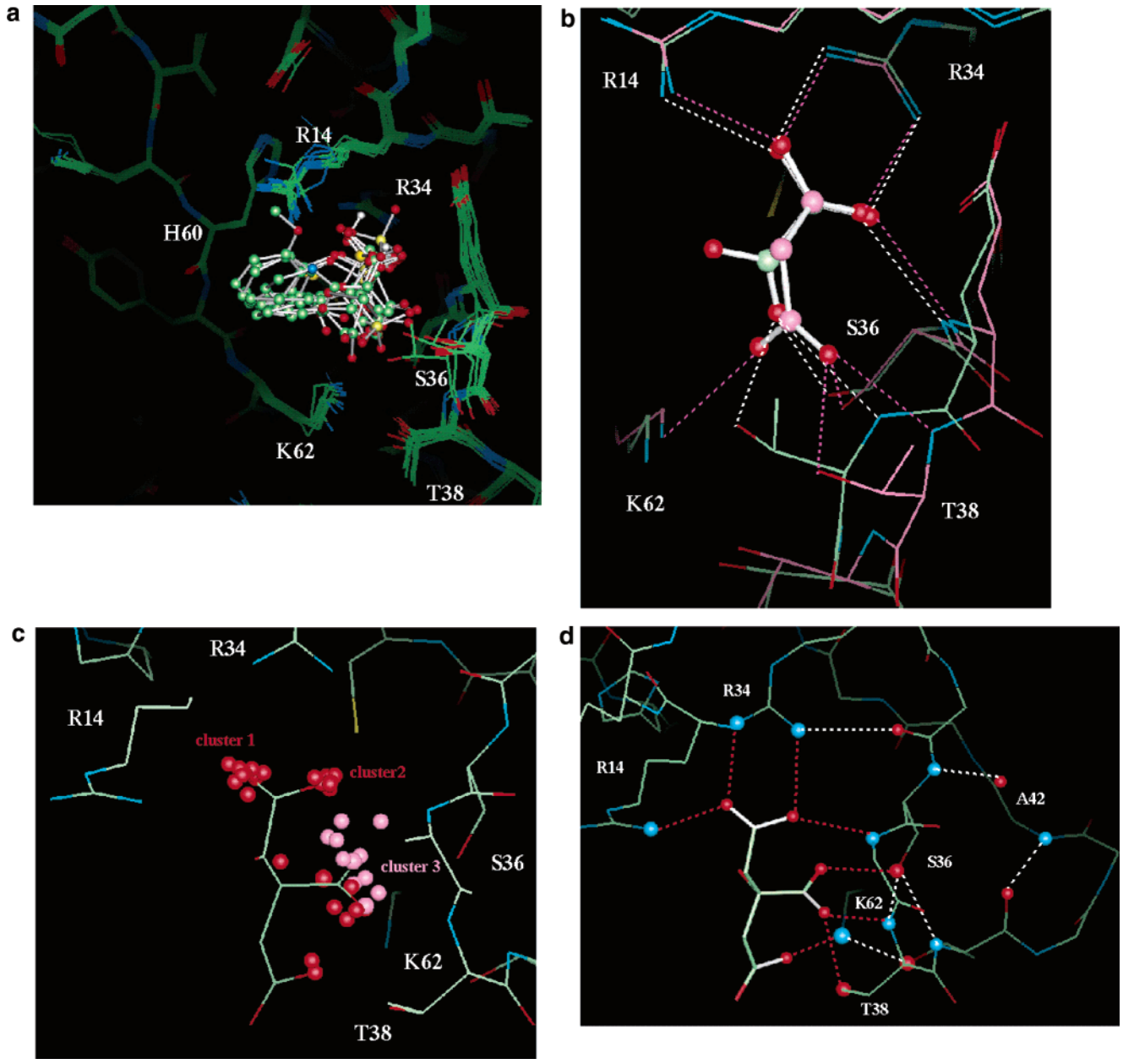

Figure 2. (a) Superposition of X-ray structures with fragments bound to the SH2 domain of *src*. (b) The binding mode of oxalate (white) and malonate (pink) in the complex with the SH2 domain of *src*. (c) The superposition of the fragment H-bond acceptors shows that they form well defined clusters when interacting with rigid protein parts (red) and less well defined clusters when interacting with flexible protein parts (pink). For easier orientation only the full structure of the citrate complex is displayed. (d) Citrate is bound in a complex H-bond network to the SH2 domain involving a total of seven H-bonds and salt-bridges indicated in red. The H-bonds stabilizing the conformation of loop 36−42 are shown in white

In the particular case of SH2, however, purely computer-based approaches have limitations in proposing new phospho-tyrosine mimics because the phospho-tyrosine binding pocket displays a high flexibility. Even in the best case, computational methods could have picked up only compounds with binding modes characterized by a pharmacophore closely related to the phosphate when using X-ray structures with phospho-tyrosine peptides as templates. Surprisingly, two out of the six fragments proposed by the program LUDI were predicted correctly. The binding of oxalate and malonate was successfully predicted using a structure containing a phospho-tyrosine peptide. However, only the salt-bridge to the rigid arginines 14 and 34 was correctly proposed while the interactions with the flexible loop were not correctly predicted. In addition, the superposition of the X-ray structures suggests that the positions of the H-bond acceptors are not as well defined as a program such as Grid would have predicted and that the distances between functional groups in the pharmacophor model are not as restrained as usually is assumed in computer-based approaches.

Our experiments show that neither ligand affinity nor the exact positioning of functional groups within the pharmacophore are an essential requirement for fragment binding and thus good selection criteria for polar fragments to the SH2 domain. However, it is important that the fragments complete the H-bond network within the phospho-tyrosine pocket. The importance of the H-bond network is highlighted by the significantly lower

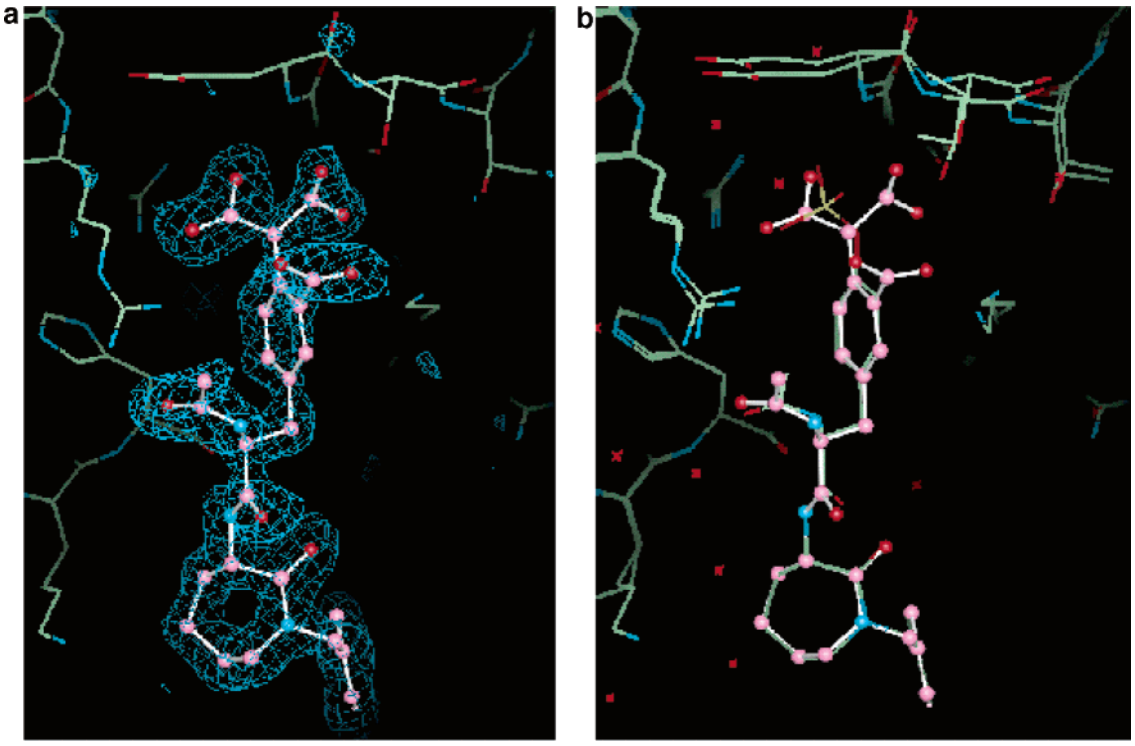

Figure 3. (a) Omit electron density map of inhibitor 2 contoured at 3σ. (b) Superposition of the X-ray structures of inhibitors 1(white) and 2 (pink) bound to the SH2 domain.

Table 1. X-ray Data for Complexes of the SH2 Domain

compound	resolution [nm]	R_{merge} [%]	R_{factor} [%]
	With Fragments		
fragment 1	0.180	8.6	17.7
fragment 2	0.155	4.8	19.1
fragment 3	0.160	9.5	18.2
fragment 4	0.160	3.5	20.9
fragment 5	0.170	6.8	20.2
fragment 6	0.190	9.8	16.9
fragment 7	0.170	4.4	17.9
fragment 8	0.150	3.2	19.0
fragment 9	0.170	6.5	18.7
fragment 10	0.185	8.1	17.6
fragment 11	0.200	5.6	18.5
fragment 12	0.200	9.9	16.4
fragment 13	0.155	5.0	19.9
fragment 14	0.225	6.7	15.6
fragment 15	0.175	4.0	20.7
fragment 16	0.165	5.0	20.7
fragment 17	0.170	6.1	18.7
fragment 18	0.155	4.2	19.3
	With Inhibitors		
inhibitor 1	0.170	6.8	19.2
inhibitor 2	0.170	4.5	19.0
inhibitor 3	0.180	7.7	20.0
inhibitor 4	0.200	7.7	19.2
inhibitor 5	0.180	7.7	19.2
inhibitor 6	0.155	5.4	19.4
inhibitor 7	0.150	5.5	19.6
inhibitor 8	0.150	5.1	20.2
inhibitor 9	0.185	5.0	19.6
inhibitor 10	0.150	5.5	19.6

affinity of full length inhibitors which form incomplete H-bond networks within the phospho-tyrosine pocket. This is also true for the phospho-tyrosine mimics described in the literature such as carboxymethylphenylalanine[28] which lack a H-bond acceptor to S36OG. Benzylmalonates[29] do not seem to be able to position their H-bond acceptors within the required limits. Recently, it was shown, that phenylmalonates related to inhibitor **2**[30] and bisphosphonates[23] maintained their activity compared to their phospho-tyrosine analogues if the correct scaffold is attached. Both compound classes are able to complete the H-bond network. The bisphosphonates were even designed to mimic the interaction of the citrate bound in the phospho-tyrosine pocket.[23]

Even though complex H-bond networks between inhibitors and proteins have been extensively described in the literature, the number of made H-bonds was emphasized rather than the number of uncompensated H-bonds. However, the importance of a complete H-bonding network has been highlighted for other biological systems. It has been shown that there is a correlation between uncompensated protein H-bonds and the buried surface area of hydrophobic atoms in high resolution X-ray structures. This correlation was successfully used to predict the stability and structure of proteins.[31] Recently, a term was introduced in a scoring function for protein−protein interactions which penalizes buried charged groups that do not form stabilizing hydrogen bonds.[32] The importance of a complete H-bond network in nucleotide recognition has been investigated. It was proposed that the correct codon:anticodon duplexes are those whose formation and interaction with the ribosomal decoding center are not accompanied by uncompensated losses of H-bonds.[33]

The experiments described above have limitations in identifying hydrophobic fragments. Hydrophobic interactions are nondirectional and fragments not exactly matching the shape of the pocket can bind in a multitude of different conformations unless they have a functional group which form directional interactions such as H-bonds with the protein. For this and experimental reasons such as limited solubility, it seems that it might be difficult to identify hydrophobic fragments and their binding modes using protein crystallography.

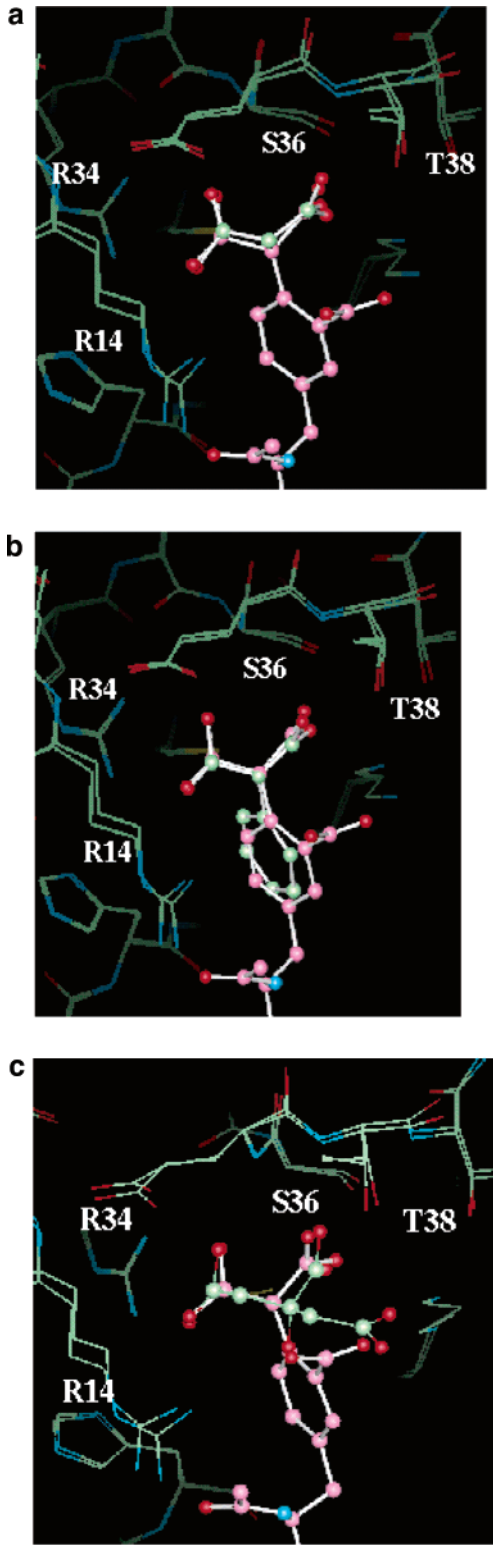

Figure 4. (a) Superposition of the X-ray structures of inhibitor **2** (pink) and (a) fragment 3 **(**malonate), (b) fragment 6 (phenylmalonate) and (c) fragment 2 (citrate) bound to the SH2 domain of *src*.

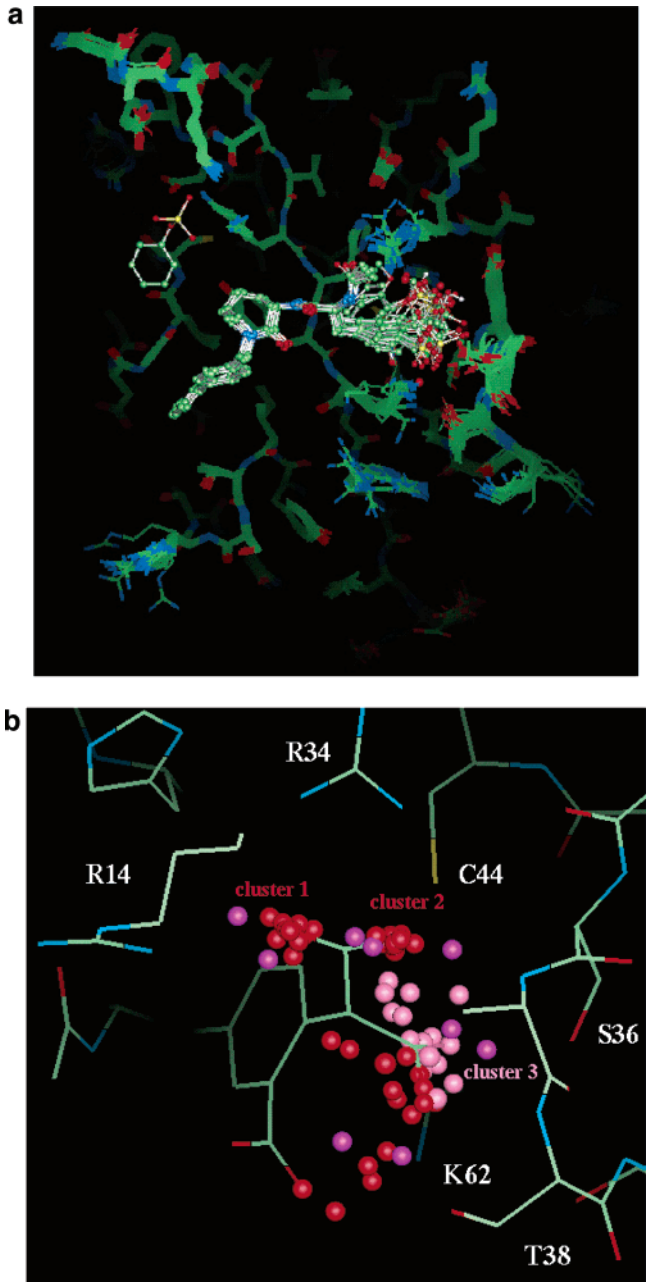

Figure 5. (a) Superposition of all X-ray structures of 18 fragments and 10 full length inhibitors based on inhibitor **1**. (b) Superposition of the H-bond acceptors of the 18 fragments and 10 full length inhibitors show that most acceptors are located within the clusters defined by the fragments shown in Figure 2a. The H-bond acceptor positions of the low affinity H-bond inhibitors 9 and 10 are indicated in purple. For easier orientation, only the protein structure of the complex with inhibitor **12** is displayed.

Our results suggest that a screen using protein crystallography might be best used in identifying inhibitor fragments for hydrophilic recognition sites. These include the phosphate binding sites in phosphatases or SH2 domains, the catalytic triad of esterases and proteases and the ATP binding site in kinases. Family members sharing the same fold usually have highly conserved recognition sites. Recognition fragments identified for one particular family member should have, therefore, a significant probability to fit into the recognition sites of other family members. Currently, there are more than 200 sequences of human SH2 domains in the SMART database.[34] They represent putative targets implicated in breast and colon cancer, T-cell activation, and osteoporosis. Some of the phosphotyrosine mimics described here will only bind if the flexibility of loop 36−42 induced by the side chain of S36 is present. Sequence alignment shows that these residues belong to the most highly conserved residues

within the SH2 domains,[34] indicating that a substantial number of other SH2 domains should display similar flexibility and bind the fragments identified for the *src*-SH2 domain. Other structures of SH2 domains deposited in the Brookhaven database[20] confirm that the structure of the recognition site is highly conserved. Examples include: the SH2 domains of tyrosine phosphatases such as syp (1aya) and shp-2 (2shp), kinases such as tyrosine kinase Fyn and cell kinase Hck (1adp5), and other proteins such as the xlp protein sap (1diz) which has been proposed to regulate the recruitment of SH2 signaling proteins to specific docking sites.

The huge number of new targets coming from genomics has made the fast turnover of projects into a competitive issue within the pharmaceutical industry. The recycling of general recognition fragments for a particular protein family identified by a protein crystallography-based screening should result in a significant speed-up of the lead generation and optimization process.

Experimental Section

General. Analytical data were recorded for the compounds described using the following general procedures. Proton NMR spectra were recorded on a Bruker AC 300 MHz spectrometer, and chemicals shifts were recorded in ppm (δ) from an internal tetramethylsilane standard in dimethyl sulfoxide-d_6 unless otherwise specified. Coupling constants (J) were recorded in hertz. Mass spectra (MS) were recorded on an MS platform (micromass) and MS Autospec TOF (micromass) in electron impact, electrospray, and chemical ionization modes. Flash chromatography was performed on silica gel 60H (Merck) using the solvent systems indicated below. For mixed-solvent systems, the volume ratios are given. Analytical HPLC was performed on a Merck HPLC system equipped with a Merck Hitachi L-4000A UV detector and reversed-phase C18 column, kromasil 5 μm. All reactions were performed under a nitrogen atmosphere using magnetic stirring. Reactions were monitored by thin-layer chromatography (TLC) on precoated plates of silica gel 60F254 (layer thickness, 0.25 mm; E. Merck, Darmstadt). Anhydrous magnesium sulfate ($MgSO_4$) was used routinely to dry the combined organic layers from extractions. Solvent was routinely removed in vacuo using rotary evaporator followed by evacuation with a vacuum pump. Methyl 2-acetamidoacrylate was purchased from Aldrich. Commonly used abbrevations are EtOAc (ethyl acetate), MeOH (methanol), DMF (*N*,*N*-dimethylformamide), THF (tetrahydrofuran), and CH_2Cl_2 (dichloromethane).

Fluoropropanedioic Acid, 4-Iodo-2-(methoxycarbonyl)phenyl-, Bis(1,1-dimethylethyl) Ester (12). An amount of 2.0 g (4.20 mmol) of 2-(4-iodo-2-methoxycarbonylphenyl)-propanedioic acid, 1,3-bis(1,1-dimethylethyl) ester **11**[9] was dissolved in 88 mL of THF. The solution was cooled to −78 °C, and then 3.35 g (16.78 mmol) of potassium hexamethyldisilazide 95% was added. The solution was stirred for 1 h under argon to −70 °C. An amount of 5.23 g (16.77 mmol) of *N*-fluorobenzenesulfonimide was added. The mixture was stirred for 15 min at −70 °C and then warmed to RT and stirred for 2 h. The mixture was poured into a saturated aqueous solution of NaCl and extracted with EtOAc. The organic extracts were washed with brine, dried, and evaporated to dryness to afford 5.54 g of crude **12** as a cream powder. Flash chromatography (320 g silica, CH_2Cl_2/EtOAc, 99:1) gave 1.74 g (83.7%) of **12** as a colorless oil. R_f = 0.20 (SiO_2F_{254}-Merck60 CH_2Cl_2/MeOH, 99/1); NMR ($CDCl_3$) δ 1.48 (s, 18H), 3.88 (s, 3H), 7.28 (d, 1H), 7.84 (d, 1H), 8.30 (d, 1H).

Fluoropropanedioic Acid, 4-[2-(Acetylamino)-2-carboxyethenyl]-2-(methoxycarbonyl)phenyl-, Bis(1,1-dimethylethyl) Ester (13b). An amount of 1.72 g (3.4 mmol) of **12** was introduced into a 500 mL flask and dissolved in 65 mL of CH_3CN. An amount of 1 g (6.95 mmol) of methyl 2-acetamidoacrylate was added to the mixture followed by 0.61 mL (4.35 mmol) of triethylamine, 45.15 mg (0.20 mmol) of Pd-$(OAc)_2$, and 0.105 mg (0.348 mmol) of tri-*o*-tolylphosphine. The suspension was refluxed for 17 h and then brought to room temperature. The suspension was poured into a saturated aqueous solution of $NaHCO_3$ and extracted with EtOAc. The organic extracts were washed with brine, dried, and evaporated to dryness to afford 2.65 g of crude **13a** as yellow oil. Flash chromatography (265 g silica, CH_2Cl_2/MeOH, 97.5/2.5) gave 0.317 g (18%) **13a** as an orange oil (mixture *Z*/*E* 50/50). R_f = 0.19 (SiO_2F_{254}Merck60 CH_2Cl_2/MeOH, 97.5/2.5); NMR ($CDCl_3$), δ 1.52 (s, 18H), 2.16 (s, 1H), 3.84 (s, 3H), 3.87 (s, 3H), 7.07 (1s, 1H), 7.37 (1s, 1H), 7.40 (d, 1H), 7.54 (dl, 1H), 7.95 (sl, 1H). Compound **13a** (0.3 g, 0.6 mmol) was dissolved in 12.2 mL THF and treated with a solution of 32.5 mg (0.774 mmol) of LiOH.H2O in 4 mL of H_2O. The resulting yellow solution was stirred for 18 h at room temperature and then poured into 25 mL of H_2O and 10 mL of 1 M HCl and extracted with EtOAc. The organic extracts were washed with brine, dried, and concentrated under vacuum to afford 0.265 g of **13b** as a cream-colored foam (90%). R_f = 0.14 (SiO_2F_{254}Merck60 CH_2Cl_2/MeOH, 90/10);MS *m*/*z* 494 $(M - H)^-$, 518 $(M + Na)^+$.

Fluoropropanedioic Acid, [4-[2-(Acetylamino)-3-[[(3*S*)-1-[[(1,1-biphenyl)-4-yl]methyl-hexahydro-2-oxo-1*H*-azepin-3-yl]amino]-3-oxo-1-propenyl]-2-(methoxycarbonyl)phenyl]-, Bis(1,1-dimethylethyl) Ester (15). An amount of 0.265 g (0.535 mmol) **13b** was dissolved in 7.6 mL of CH_2Cl_2 and 2.55 mL of DMF in a 50 mL flask under argon and cooled in an ice bath. An amount of 0.102 g (0.535 mmol) of 1-(3-dimethylaminopropyl)-3-ethylcarbodiimide hydrochloride (EDCI) was added followed by 0.072 mg (0.535 mmol) of 1-hydroxybenzotriazole (HOBT). The solution was stirred at room temperature for 15 min and then added dropwise to a cooled solution of 0.232 mg (0.535 mmol) of amine (3*S*)-amino-1-[[(1,1′-biphenyl)-4-yl]methyl]hexahydro-2*H*- azepin-2-one **14**[13] and 0.185 mL (1.07 mmol) of *N*,*N*-diisopropylethylamine in 5 mL of CH_2Cl_2 (0 °C). The resulting solution was stirred for 5 h at room temperature and then poured into H_2O and extracted with EtOAc. The organic extracts were washed with an aqueous solution of $NaHCO_3$ and then brine, dried, and concentrated to afford 0.391 g of crude product. Flash chromatography (50 g of silica, CH_2Cl_2/MeOH, 90/10) gave 0.275 g of the expected compound as a white foam (67%). R_f = 0.13 (SiO_2F_{254}Merck60 CH_2Cl_2/MeOH, 97.5/2.5); MS *m*/*z* 770 $(M - H)^-$,794 $(M + Na)^+$.

Fluoropropanedioic Acid, [4-[2-(Acetylamino)-3-[[(3*S*)-1-[[(1,1-biphenyl)-4-yl]methyl-hexahydro-2-oxo-1*H*-azepin-3-yl]amino]-3-oxo-1-propenyl]-2-(methoxycarbonyl)phenyl]- (4). A hydrogenating flask was charged with 0.264 g (0.342 mmol) of **15** and dissolved in 30 mL of methanol, and 85 mg of 10% palladium on carbon (E10ND charge 7389) was added. The mixture was placed under 1760 mbar of hydrogen for 48 h, and then the suspension was filtered over Celite and concentrated to afford 0.241 g of the pure hydrogenated intermediate as a white foam (91%, 60/40 mixture of diastereoisomers). R_f = 0.44 (SiO_2F_{254}Merck60 CH_2Cl_2/MeOH, 96.5/3.5) HPLC (CH_3CN/H2O, 75:25, 0.01%,TFA, 1 mL/min, 63 bar, 230 nm, 9.45 min, 92.5%; NMR (DMSO-d_6) δ 1.17−1.67 (m, 2H), 1.3−1.9 (m, 4H), 1.46 (s, 18H), 1.75 (1s, 3H), 1.76 (1s, 3H), 2.81 and 3.06 (2d, 1H), 2.81 and 3.06 (2dd, 1H), 3.28 and 3.58 (2m, 2H), 3.75 (s, 3H), 4.60−4.67 (m, 1H), 4.61 (s, 1H), 4.52 and 4.69 (d, 1H), 4.47 and 4.72 (d, 1H), 7.19, 7.36, 7.46, 7.65, 7.54, 7.75 (12H), 8.20 (dd, 1H), 8.24 (dd, 1H). 0.204 g (0.264 mmol) of this material was dissolved in 6 mL of 98% HCOOH (157 mmol). The solution was stirred for 6 h at room temperature and then poured into H_2O and extracted with AcOEt. The organic extracts were washed with an aqueous solution of $NaHCO_3$ and then brine, dried, and concentrated to afford 0.187 g of crude **4** as a white foam. Crude **4** was triturated with cold diethyl ether and filtered to afford 0.156 g (96%) of **4** as a white powder (60/40 mixture of diastereoisomers). R_f = 0.13 (SiO_2F_{254}Merck60 CH_2Cl_2/MeOH/AcOH, 80/20/5). NMR (MeOD), δ 1.23−1.86 ((m, 6H), 1.94−1.96 (s, 3H), 2.96−3.40 (d, 2H), 3.37 and 3.59 (dd, 2H), 3.81 (s, 3H), 4.57

and 4.72 (m, 2H), 4.66 (m, 1H), 7.28−7.65 (m, 1H), 7.73−7.78 (m, 11H), 7.93 (m, 1H), 8.10 (m, 1H), 8.30 (m, 1H). MS *m/z* 660 $(M - H)^-$, 662 $(M + H)^+$.

Carbamic Acid, [(1*S*)-2-[[(3*S*)-1-([1,1′-Biphenyl]-4-ylmethyl)hexahydro-3-methyl-2-oxo-1*H*-azepin-3-yl]amino]-1-[[3,4-bis(diethoxyphosphinyl)phenyl]methyl]-2-oxoethyl]-, 1,1-Dimethylethyl Ester (17). An amount of 0.3 g (0.56 mmol) of 3,4-bis(diethoxyphosphinyl)-*N*-[(1,1-dimethylethoxy)carbonyl]-L-phenylalanine **16**[23] was dissolved in 6 mL of CH_2Cl_2 and 0.6 mL of DMF in a 50 mL flask under argon and cooled in an ice bath. An amount of 0.106 g (0.558 mmol) of 1-(3-dimethylaminopropyl)-3-ethylcarbodiimide hydrochloride (EDCI) was added followed by 0.075 mg (0.558 mmol) of 1-hydroxybenzotriazole (HOBT). The solution was stirred for 15 min at room temperature and then added dropwise to a cooled solution of 0.140 mg (0.558 mmol) of **14**.[13] The resulting solution was stirred for 2 h at room temperature and then poured into H_2O and extracted with CH_2Cl_2. The organic extracts were washed with an aqueous solution of $NaHCO_3$ and then brine, dried, and concentrated to afford 0.300 g of crude **17**. Flash chromatography (30 g of silica, CH_2Cl_2/MeOH, 95/5) gave 0.260 g of **17** (57%). $R_f = 0.37$ (SiO_2F_{254}Merck60 CH_3COCH_3/ACOEt/H_2O, 50/40/10); MS *m/z* 812 $(M - H)^-$, NMR ($CDCl_3$), δ 1.36 (m,12H), 1.14−2.12 (m, 6H), 3.10 (m, 1H), 3.27 (m, 2H), 3.51 (dd, 1H), 4.20 (m, 8H), 4.51 (m, 1H), 4,55 and 4.75 (dd, 2H), 4.63 (dd, 1H), 4.94 (d, 1H), 7.30 and 7.56 (m, 4H), 7.35 (m, 1H), 7.44 (dd, 1H), 7.47 (dd, 1H), 7.57 (dd, 1H), 7.96 (dd, 1H), 8.08 (dd, 1H).

Phosphonic Acid, [4-[(2*R*)-2-(Acetylamino)-3-[[(3*S*)-1-([1,1′-biphenyl]-4-ylmethyl)hexahydro-3-methyl-2-oxo-1*H*-azepin-3-yl]amino]-3-oxopropyl]-1,2-phenylene]bis, Tetraethyl Ester (18b). An amount of 0.24 g (0.294 mmol) of**17** was dissolved in 4 mL of CH_2Cl_2 and 1.5 mL of trifluoroacetic acid in a 50 mL flask under argon. The mixture was stirred for 1 h at room temperature and then concentrated under reduced pressure. The residue was dissolved in CH_2Cl_2 and washed with an aqueous solution of $NaHCO_3$ and then brine, dried, and concentrated to afford 0.200 g of the amine **18a** (95%). $R_f = 0.33$ (SiO_2F_{254}Merck60 CH_2Cl_2/MeOH, 90/10); MS *m/z* 712 $(M - H)^-$. An amount of 0.20 g (0.28 mmol) of **18a** was dissolved in 4 mL of pyridine under argon and cooled at 0 °C, and then 0.027 mL (0.336 mmol) of acetic anhydride was added dropwise. The resulting solution was stirred for 2 h at room temperature and then poured into H_2O and extracted with CH_2Cl_2. The organic extracts were washed with an aqueous solution of $NaHCO_3$ and then brine, dried, and concentrated to afford 0.200 g of crude product. Flash chromatography (20 g of silica, CH_2Cl_2/MeOH, 95/5) gave 0.170 g of **18b** (81%). $R_f = 0.46$ (SiO_2F_{254}Merck60 CH_2Cl_2/MeOH, 90/10); MS *m/z* 754$(M - H)^-$. NMR ($CDCl_3$),δ 1.20 (m, 1H), 1.34−1.37 (t, 12H), 1.47 (m, 1H), 1.73 (m, 2H), 1.92 (m, 1H), 2.00 (s, 3H), 2.03 (m, 1H), 3.12 (dd, 1H), 3.27 (dd, 1H), 3.28 (m, 1H), 3.52 (dd, 1H), 4.19 (m, 8H), 4,61 and 4.70 (d, 2H), 4.61 (m, 1H), 4.81 (dd, 1H), 6.05 (d, 1H), 7.33 and 7.57 (m, 7H), 7.41 (m, 1H), 7.44 (m, 3H), 7.96 (dd, 1H), 8.07 (dd, 1H).

[4-[(2*R*)-2-(Acetylamino)-3-[[(3*S*)-1-([1,1′-biphenyl]-4-ylmethyl)hexahydro-3-methyl-2-oxo-1*H*-azepin-3-yl]amino]-3-oxopropyl]-1,2-phenylene]bisphosphonic Acid (9). An amount of 0.165 g (0.218 mmol) of**18b** was dissolved in 3.3 mL of CH_2Cl_2 in a 25 mL flask under argon and cooled in an ice bath, and then 0.290 mL (2.18 mmol) of iodotrimethylsilane was added. The resulting solution was stirred for 3 h, warmed to room temperature, and finally concentrated under reduced pressure. This material was dissolved in MeOH, concentrated under reduced pressure, and filtered to afford 0.130 g of crude **9**. Preparative HPLC (CH_3CN/H_2O, 75:25, 0.01%,TFA, 3 mL/min, 95 bar, 230 nm gave 0.070 g of **9** (50%); MS *m/z* 642 $(M - H)^-$; NMR (DMSO-d_6) δ 1.17 (m, 1H), 1.45 (1H), 1.68 (dl, 2H), 1.82 (m, 2H), 1.79 (s, 3H), 2.82 (dd, 1H), 3.19 (dd, 1H), 3.28 (dd, 1H),3.60 (dd, 1H), 4.52 (dd, 1H), 4.60 (m, 1H), 4.69 (dd, 1H), 7.37 and 7.63 (dd, 4H), 7.37 (m, 1H), 7.46 (t, 2H), 7.54 (d, 1H), 7.65 (d, 1H), 7.82 (m, 1H), 7.89 (m, 1H), 8.23 (m, 2H).

Acknowledgment. The authors would like to thank Herman Schreuder, Steve Lindell, and Klaus Haaf for helpful discussion and Alexander Liesum for excellent technical assistance. This work was done during the course of a collaboration with ARIAD Pharmaceuticals and we are grateful to T. Sawyer and M. Hatada for stimulating discussions.

Supporting Information Available: ^1H NMR spectra of compounds **4** and **9**. This material is available free of charge via the Internet at http://pubs.acs.org.

References

(1) Spencer, R. W. High-throughput screening of historic collections: observations on file size, biological targets, and file diversity. *Biotechnol. Bioeng.* **1998**, *61*, 61−67.
(2) Kuntz, I. D.; Blaney, J. M.; Oatley, S. J.; Langridge, R.; Ferrin, T. E. A geometric approach to macrormolecule-ligand interactions. *J. Mol. Biol.* **1982**, *161*, 269−88.
(3) Rarey, M.; Kramer, B.; Lengauer, T.; Klebe, G. A fast flexible docking method using an incremental construction algorithm. *J. Mol. Biol.* **1996**, *261*, 470−489.
(4) Goodford, P. J. A. Computational Procedure for determining energetically favorable binding sites on biologically important interaction sites. *J. Med. Chem.* **1985**, *28*, 849−857.
(5) Boehm, H. J., The computer program LUDI: a new method for the de novo design of enzyme inhibitors. *J. Comput.-Aided Mol. Des.* **1992**, *6*, 61−78.
(6) Shuker, S. B.; Hajduk, P. J.; Meadows, R. P.; Fesik, S. W. Discovering high-affinity ligands for proteins: SAR by NMR. *Science* **1996**, *274*, 1531−4.
(7) Hajduk P. J.; Zhou, M.-M.; Fesik; S. W. NMR-based discovery of phosphyotyrosine mimetics that bind to the Lck SH2 domain. *Bioorg. Med. Chem. Lett.* **1999**, *9*, 2403−2406.
(8) Nienaber; V. L.; Richardson, P. L. Klighofer, V.; Bouska, J. J.; Giranda, V. L.; Greer; J. Discovering novel ligands for macromolecules using X-ray crystallography screening. *Nat. Biotechnol.* **2000**, 18, 1105−1107.
(9) Lesuisse, D.; Lange, G.; Deprez, P.; Schoot, B.; Benard, D.; Delettre, G.; Marquette, J.-P.; Broto, P.; Jean-Baptiste, V.; Bichet, P.; Sarubbi, E.; Mandine, E. J. SAR and X-ray- a new approach combining fragment-based screening and rational drug design: Application to the discovery of nanomolar inhibitors of src SH2. *J. Med. Chem.* **2002**, *45*, 2379−2387.
(10) Soriano, P.; Montgomery, C.; Geske, R.; Bradley, A., Targeted disruption of the c-src proto-oncogene leads to osteopetrosis in mice. *Cell* **1991**, *64*, 693−702.
(11) Waksman, G.; Shoelson, S. E.; Pant, N.; Cowburn, D.; Kuriyan, J. Binding of a high affinity phosphotyrosyl peptide to the src sh2 domain: crystal structures of the complexed and peptide-free form. *Cell* **1993**, *72*, 779−790.
(12) Deprez, P.; Mandine, E.; Gofflo; D.; Meunier, S.; Lesuisse, D. Small ligands interacting with the phospho-tyrosine binding pocket of the Src SH2 protein. *Bioorg. Med. Chem. Lett.* **2002**, *12*, 1295−1298.
(13) Deprez, P.; Baholet, I.; Burlet, S.; Lange, G.; Schoot, B.; Vermond, A.; Mandine, E.; Lesuisse, D. Discovery of highly potent Src SH2 binders: Structure−Activity studies and X-ray structures. *Bioorg. Med. Chem. Lett.* **2002**, *12*, 1291−1294.
(14) Lesuisse, D.; Deprez, P.; Albert, E.; Duc, T. T.; Sortais, B.; Gofflo, D.; Jean-Baptiste, V.; Marquette, J.-P.; Schoot, B.; Sarubbi, E.; Lange, G.; Broto, P.; Mandine, E. Discovery of Thioazepinone Ligands for Src SH2: From Nonspecific to Specific Binding. *Bioorg. Med. Chem. Lett.* **2001**, *11*(16), 2127−2131.
(15) Lange, G.; Lesuisse, D.; Deprez.; P.; Schoot, B.; Loenze, P.; Bénard, D.; Marquette, J.-P.; Broto, Sarubbi, E.; Mandine, E. Principles governing the binding of a class of nonpeptidic inhibitors to the SH2 domain of src studied by X-ray analysis. *J. Med. Chem* **2002**, *45*, 2915−2922.
(16) Kabsch, W., Automatic processing of rotation diffraction data from crystals of initially unknown symmetry and cell constants. *J. Appl. Crystallogr.* **1993**, *26*, 795−800.
(17) Brunger, A. T.; Kurkowski, A.; Erickson, J. W. Slow-cooling protocols for crystallographic refinement by simulated annealing. *Acta Crystallogr.* **1990**, *A46*, 46−57.
(18) Oldfield, T. J. A number of real-space torsion-angle refinement techniques for proteins, nucleic acids, ligands and solvent. *Acta Crystallogr. D* **2001**, *D57*, 82−94.
(19) W. Kabsch. A discussion of the solution for the best rotation to relate two sets of vectors. *Acta Crystallogr.* **1978**, *A34*, 827−828.
(20) Berman H. M. et al. The protein data bank. *Nucleic Acids Res.* **2000**, *28*, 235−242.
(21) Deprez, P.; Lesuisse, D.; Bénard, D.; Caprolactam derivatives and uses thereof. WO 01/68655 A2, 2001.

(22) Kawahata, N.; Yang, M. Y.; Luke, G. P.; Shakespeare, W. C.; Sundaramoorthi, R.; Wang, Y.; Johnson, D.; Merry, T.; Violette, S.; Guan, W.; Bartlett, C.; Smith, J.; Hatada, M.; Lu, X.; Dalgarno, D. C.; Eyermann, C. J.; Bohacek, R. S.; Sawyer, T. K. A novel phosphotyrosine mimetic 4′-carboxymethyloxy-3′-phosphonophenylalanine (Cpp): exploitation in the design of non peptide inhibitors of pp60src SH2 Domain. *Bioorg. Med. Chem. Lett.* **2001**, *11*, 2319−23.

(23) Shakespeare, W. et al. Structure-based design of an osteoclast-selective, nonpeptide src homology 2 inhibitor with in vivo antiresorptive activity. *Proc. Natl. Acad. Sci.* **2000**, *97*, 9373−9378.

(24) Maly, D. J.; Choong, I. C.; Ellman, J. A. Combinatorial target-guided ligand assembly: identification of potent subtype-selective c-Src inhibitors. *Proc. Natl. Acad. Sci. U.S.A.* **2000**, *97*, 2419−2424.

(25) Kelly, M. A. et al. Characterization of SH2−Ligand Interactions via Library Affinity Selection with Mass Spetrometric Detection. B*iochemistry* **1996**, 35, 11747−11755.

(26) Hajduk, P. J.; Meadows, R. P.; Fesik, S. W. Privileged molecules for protein binding identified from NMR-based screening. *J. Med. Chem.* **2000**, *43*, 3443−3447.

(27) Grueneberg, S.; Wendt, B.; Klebe, G. Subnanomolar Inhibitors from Computer Screening: A model study using Human Carbonic Anhydrase II *Angew. Chem., Int. Ed.* **2001**, *40*, 389−393.

(28) Tong, L.; Warren, T. C.; Lukas; S.; Schembri-King, J.; Betageri, R.; Proudfoot, J.; Jakes, S. Carboxymethyl-phenylalanine as a replacement for phospho-tyrosine in SH2 domain binding *J. Biol. Chem.* **1998**, *273*, 20238−20242.

(29) Charifson, P. S. et al. Peptide Ligands of pp60c-src SH2 domains: a thermodynamic and structural study. *Biochemistry* **1997**, *36*, 6283−6293.

(30) Gao, Y.; Wu, L.; Luo, J.; Guo, R.; Jang, D.; Zhang, Z.-Y.; Burke, T. Examination of novel nonphosphorous-containing phosphotyrosyl mimetics against protein-tyrosine phosphatase 1B and demonstration of differential affinities toward Grb2 SH2. *Bioorg. Med. Chem. Lett* **2000**, *10*, 923−927.

(31) Savage, H. J.; Elliott, C. J.; Freeman, C. M. Finney, J. L. Lost Hydrogen bonds and buried Surface Area: Rationalizing stability in globular proteins. *J. Chem. Soc., Faraday Trans.* **1993**, *89*, 2609−17.

(32) Norel.; R:, Sheinerman, F.; Petrey, D.; Honig, B. Electrostatic contributions to protein−protein interactions: Fast energetic filters for docking and their physical basis. *Protein Sci.*. **2001**, *10*, 2147−2161.

(33) Lim, V. I. Curran, J. F. Analysis of codon; anticodon interactions within the ribosome provides new insight into codon reading and the genetic code structure. *RNA* **2001**, *7*, 942−957.

(34) Schultz, J.; Milpetz, F.; Bork, P.; Ponting, C. P. SMART, a simple modular architecture research tool: identification of signaling domains. *Proc. Natl. Acad. Sci. U.S.A.* **1998**, *95*, 5857−5864.

JM020970S